Int J Adv Manuf Technol (2015) 81:1961–1976
DOI 10.1007/s00170-015-7338-1

ORIGINAL ARTICLE

Analysis of aluminum oxynitride AlON (Abral®) abrasive grains during the brittle fracture process using stress-wave emission techniques

Krzysztof Nadolny[1] · **Paweł Sutowski**[1] · **Daniela Herman**[2]

Received: 24 February 2015 / Accepted: 18 May 2015 / Published online: 3 June 2015

Abstract This article presents the properties of a new generation of abrasive grains made from aluminum oxynitride AlON (Abral®), as well as the methodology and application of acoustic emissions as a measurement analysis method for those stress waves generated during the brittle fracture process. The methodology of evaluation of grain properties presented in the article mostly consists of examining the resistance to fracture as a result of the force applied and analyzing the registered acoustic emission signals. The applied solution involves using a tension machine and conducting compression tests upon AlON grains and, as a point of comparison, white fused alumina 99A grains, microcrystalline sintered corundum SG™, and green silicon carbide 99C. What was analyzed were the registered compression force values and acoustic emission signals within the time and frequency domains. The characteristics within the time function involve determination of the event and ring-down parameters for single acoustic emission impulses. In the case of the frequency analysis, the signal amplitude and phase characteristics were determined. The research results indicate that stress fractures appear during grain compression tests, which generate elastic waves of various characteristics. The recording and analysis of these waves, in the form of an acoustic emission signal, turned out to be an efficient tool for analyzing the process of abrasive grain cracking and made it possible to differentiate their structure. The research results obtained point to the necessity for further analyses into stress-wave emission, especially with reference to the selection of the most effective methods for analyzing the signal frequency spectrum.

Keywords Mechanical properties · Abrasive grains · Acoustic emission · Aluminum oxynitride · So-gel alumina · White fused alumina · Silicon carbide

✉ Krzysztof Nadolny
krzysztof.nadolny@tu.koszalin.pl

Paweł Sutowski
pawel.sutowski@tu.koszalin.pl

Daniela Herman
daniela.herman@tu.koszalin.pl

[1] Department of Production Engineering, Faculty of Mechanical Engineering, Koszalin University of Technology, Racławicka 15-17, 75-620 Koszalin, Poland

[2] Subject Group of Fundamentals of Material Science and Technical Ceramics, Faculty of Technology and Education, Koszalin University of Technology, Sniadeckich 2, 75-453 Koszalin, Poland

Nomenclature

AE	Acoustic emission
GWAS	Grinding wheel active surface
SEM	Scanning electron microscope
$AE_{filt.}$	Filtered raw acoustic emission signal, V
AE_{RMS}	Root mean square value of acoustic emission signal, V
DFT_{NFFT}	The *n*-point discrete Fourier transform parameter (equal to the next power of 2 from the length of signal)
F_c	Compressive force, N
G_m	Average crystal size, μm
K_I	Stress intensity factor, MPa $m^{1/2}$
n_e	Event count rate, s^{-1}
N_e	The number of event counts
U_g	Threshold level, V

1 Introduction

The development of modern abrasive grinding processes is most often connected with the introduction of new construction

materials which generate high expectations within the industry due to their hard-to-cut nature, as well as with the development of new kinematic types of the grinding process, or the implementation of new abrasive materials.

No considerable progress has been observed in the field of new abrasive materials since the 1980s when the 3M Company (1981), and later Norton (1986), presented a new type of grain made from microcrystalline sintered corundum and obtained using the sol-gel method. It was only in 2000 when the French company Pechiney Electrometallurgy Abrasives & Refractories introduced the technology of producing aluminum oxynitride that it became possible to use this material as an abrasive grain.

Aluminum oxynitride type γ ($Al_xO_yN_z$—AlON in short) is well known as a ceramic material used in the manufacture of surfaces within the electronics industry or in the production of melting pots, among other things. It was first presented as an abrasive material by the US Secretary of the Army, US patent no. 4241000, in 1980 [1], along with a description of how to produce it. The described AlON grain production technology consisted in preparing a fine-grained mixture of the precursor's solid bodies (Al_2O_3 and AlN), followed by heat processing within an oxidation environment, and finally thickening through sintering, to the value of at least 97 % theoretical density in order to shape a regular form of aluminum oxynitride spinel.

In 1988 [2] and then in 1990 [3], the 3M Company developed and patented the technology for producing abrasive materials from Al_2O_3, aluminum oxynitride type γ, as well as metal nitrides from group IVb of the periodic table. In this case, it was suggested that abrasive grains produced using the sol-gel method with reactive sintering should be used. The high cost of the grains produced made it necessary, however, to look for other methods that would make it possible to obtain a more advantageous ratio of quality to cost.

In 1991, in France (FR 9100376), and later on, within the EU (EP 0494129), Japan (JP 04-304359), Canada (CA 2058682), and the USA (US 5314675) [4], the Pechiney Electrometallurgy Company patented the process of direct nitriding of metals that possessed a relatively low melting temperature, especially aluminum. In 1991, the same company patented a wide variety of abrasive or refractory materials on the basis of oxynitrides in France (FR 9105419), as well as the EU (EP 0509940), Canada (CA 2065821), the USA (US 5336280) [5], and Japan (JP 05-117042 A). These patents included materials made of aluminum oxynitride-type AlON, obtained through direct nitriding, melting in electric furnaces, and rapid cooling. As a result, the costs of producing such

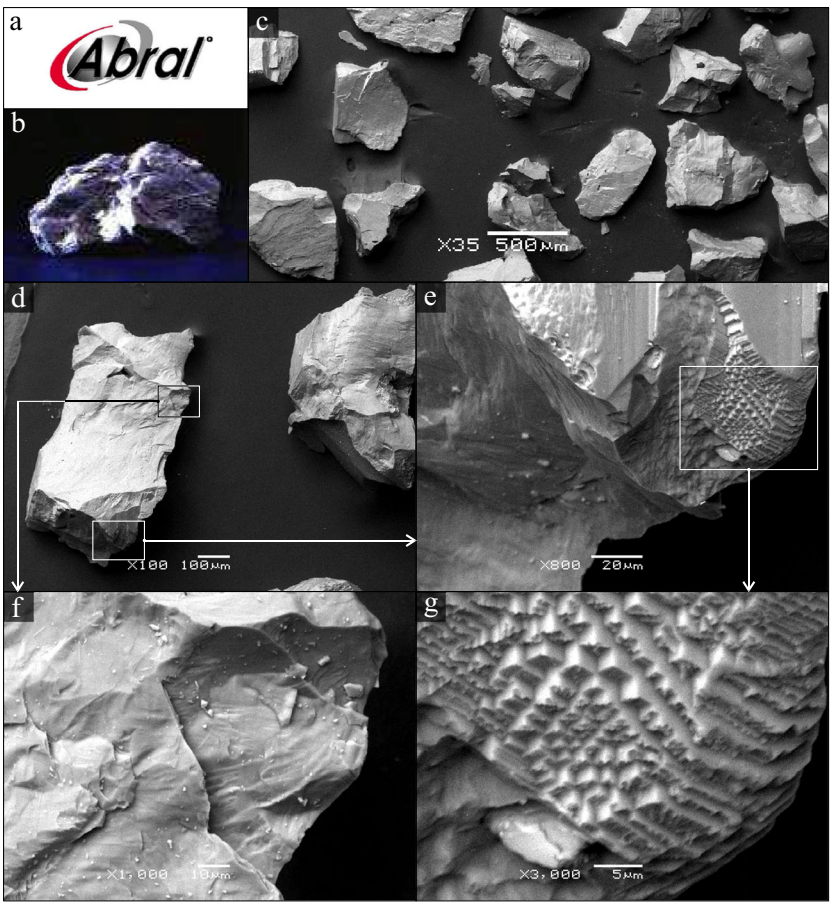

Fig. 1 Registered trademark of Abral® abrasive grains [8] (**a**), general view of the grain [8] (**b**), and SEM images of the grains number 46: magnification ×35 (**c**), magnification ×100 (**d**), magnification ×800 (**e**), magnification ×1000 (**f**), and magnification ×3000 (**g**)

abrasive grains were considerably reduced, while the grains were still characterized by the equivalent contents of AlN, which was from 11 to 12.5 %. The next step in the development of AlON grain production technology took place in 1995 when Pechiney Electrometallurgy patented in France (FR2720391) abrasive grains derived from aluminum oxynitride AlON, obtained through sintering in an electric furnace and whose hardness was increased due to dispersion of fine-grained titanium green silicon carbide crystals in the base material [6].

2 Characteristics of aluminum oxynitride abrasive grains

On basis of the technologies developed in 2000, Pechiney Electrometallurgy Abrasives & Refractories began production of abrasive grains from aluminum oxynitride under the trade name Abral® (Fig. 1). These abrasive grains were suitable for use in the manufacture of abrasive tools with ceramic and resin bond designed for precision and high-efficiency grinding [7].

The French company Pechiney Electrometallurgy was then part of the capital group Pechiney International S.A., which was taken over by Canadian Alcan Inc. in 2003. In October 2007, Alcan Inc. was bought by Rio Tinto, one of the leading extraction companies [9]. The existing structures of Rio Tinto that dealt with aluminum extraction and processing joined forces with the resources of Alcan Inc. and created the company Rio Tinto Alcan, which then transformed into a company called Alteo and now produces Abral® grains in one of its factories in La Bathie in France [8, 10].

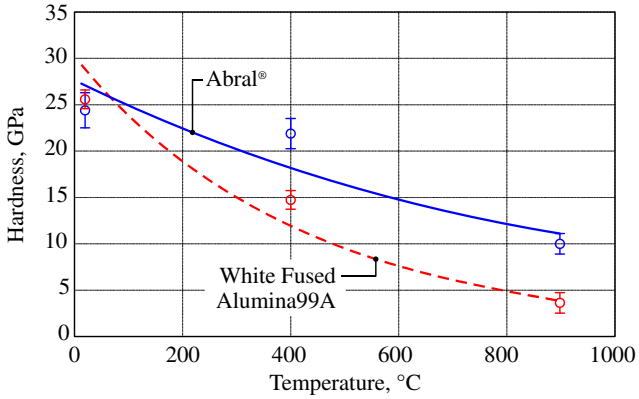

Fig. 2 Transformation of white fused alumina 99A and AlON (Abral®) abrasive grain hardness as a function of temperature [15–18]

Aluminum oxynitride abrasive grains have a polycrystalline structure (Fig. 1g) and are characterized by a slightly lower hardness and malleability compared with white fused alumina 99A (Table 1). The presence of aluminum oxynitride in AlON grains contributes to their considerably greater hardness in high temperatures as compared with 99A grains (Fig. 2).

The presence of aluminum oxynitride also prevents the AlON grains' surface from being dampened by the melted steel (Fig. 3). This results in the almost complete removal of the phenomenon of the machined material sticking to the abrasive grains' active apexes and considerably limits clogging of the grinding wheel active surface (GWAS) [17, 19–23].

Figure 4 presents the SEM images of the active surface of the single-layer electroplated grinding wheels, made from white fused alumina 99A grains (Fig. 4a), microcrystalline sintered corundum grains (Fig. 4b), and aluminum oxynitride ones (Fig. 4c), after the process of plunge

Table 1 The chemical composition and properties of the types of abrasive grain analyzed [11–14]

	White fused alumina 99A	Microcrystalline sintered corundum	Silicon carbide 99C	Abral®
Full name	Fused alumina Al_2O_3	Microcrystalline sol-gel-sintered alumina	Silicon carbide green SiCg	Aluminum oxynitride $Al_xO_yN_z$
Chemical composition (%)	Al_2O_3 99.7 SiO_2 0.01 Fe_2O_3 0.02 Na_2O 0.16 CaO+MgO 0.02	Al_2O_3 95–99 MgO/Fe_2O_3 0–5	SiC >98.5 C ~0.30 Fe ~0.02 Si ~0.03	$Al_xO_yN_z$ 99.5 SiO_2 0.06 Fe_2O_3 0.03 Na_2O 0.11
Crystal size (μm)	~10	<1	<1	~10
Shape	Pointed, sharp	Pointed, very sharp	Sharp, angular	Pointed, very sharp
Specific density (g/cm^3)	3.96	3.87	3.12–3.21	3.65
Knoop hardness HK (GPa)	20.3	21.5	24–30	18.0
Ductility (MPa m$^{1/2}$)	2.0	3.7	2.2–3.3	1.65
The critical stress intensity factor K_{Ic} (MPa m$^{1/2}$)	2.7	3.5–4.3	1.9	–
Coefficient of friction (hardened steel)	0.34	0.19	–	–
Thermal conductivity coefficient λ (W/m K)	27–35	27–35	42.5	–

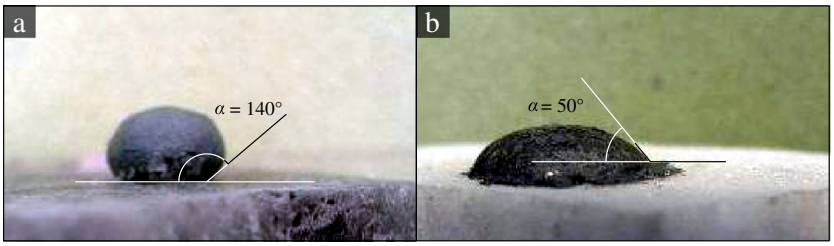

Fig. 3 Wetting of the grit by steel 100Cr6: **a** aluminum oxynitride (Abral®) and **b** white fused alumina 99A [15–18]

grinding in steel [16, 17, 24]. They indicate that the surface of the AlON grains was the only one free from the phenomenon of clogging with the machined material, while the active apexes showed a tendency to self-sharpen and unfold new sharp corners (Fig. 4c).

The described AlON grains' features make it suitable for grinding steel with a hardness ranging from 45 to 60 HRC, as well as stainless steel. These grains are highly useful in grinding processes characterized by a large surface of contact between the grinding wheel and the workpiece, in which there is the risk of thermal damage to the machined surfaces. These include, in particular, the processes of grinding with the grinding wheel spindle vertical axis, plunge grinding, deep-feed plunge grinding, centerless grinding, and crankshaft grinding [16, 17, 24].

Apart from limiting the heat stresses in the grinding zone that result from friction, reducing clogging of the GWAS also extends the tool life of diamond dressers used in the grinding wheel conditioning, sharpening, and shaping processes. This results from limiting the chemical wear of the diamond from those chips of the machined steel that find themselves on the surface of the sharpened grinding wheel surface [24].

3 Experimental investigations

The aim of the experimental tests was to evaluate the mar resistance in aluminum oxynitride grains through a compression test. The evaluation was made in relation to other popular abrasive grain types: white fused alumina 99A, microcrystalline sintered corundum SG™, and green silicon carbide 99C. A filtered acoustic emission signal was used in the tests as the main source of information on the grain decohesion process.

3.1 Methodology of the experimental tests

The experimental tests were carried out on a work stand for resistance tests, equipped with the resistance machine Tensometer type W, made by the Monsanto Company (Great Britain). The machine cooperated with measurement components made by Hottinger Baldwin Messtechnik GmbH (Germany), and these included a two-channel measurement amplifier MP85A, as well as force and track sensors that made it possible to obtain a linearity of the analog-digital processing system of greater than 0.03 %. Tensometer feed speed used in the experiments was 1.0 mm/min. There were also elements of the measurement track mounted on the stand for registering the acoustic emission signal (AE) that came from the direct proximity of the compression zone. The raw signal then underwent preprocessing using a high-pass filter (HPF=50 kHz) and a low-pass filter (LPF=1000 kHz). Figure 5 presents the general view of the research stand. What can also be observed in this view is the method of mounting the AE sensor (Fig. 5b) and the measurement machine jaw (with the abrasive grain) in the open position (Fig. 5c) and directly before beginning the test—after removing the clearance (Fig. 5d).

The most important element of the system for registering the AE signal was the piezoelectric sensor type 8152B211, made by Kistler Instrument Corporation (Switzerland). This worked in conjunction with the system of data acquisition, type PXIe-1073, made by National Instruments Corporation (USA).

In order to interpret the obtained measurements correctly, observation of grains before and after the decohesion process was carried out using an electron scanning microscope JSM-5500LV, made by JEOL Ltd. (Japan). The tests were carried

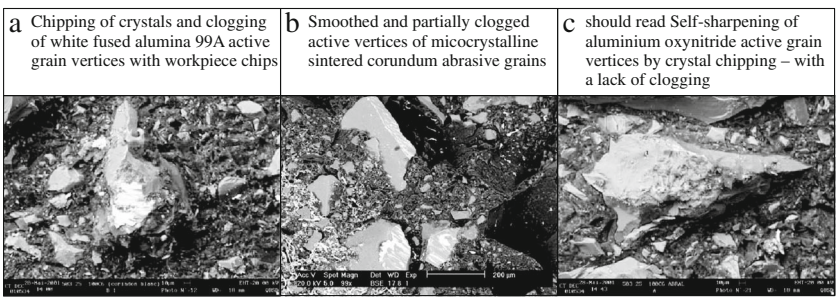

Fig. 4 Comparison of SEM images of the grinding wheel active surface made from white fused alumina 99A grains (**a**), microcrystalline sintered corundum grains (**b**), and AlON grains (**c**) after the plunge grinding process [16]

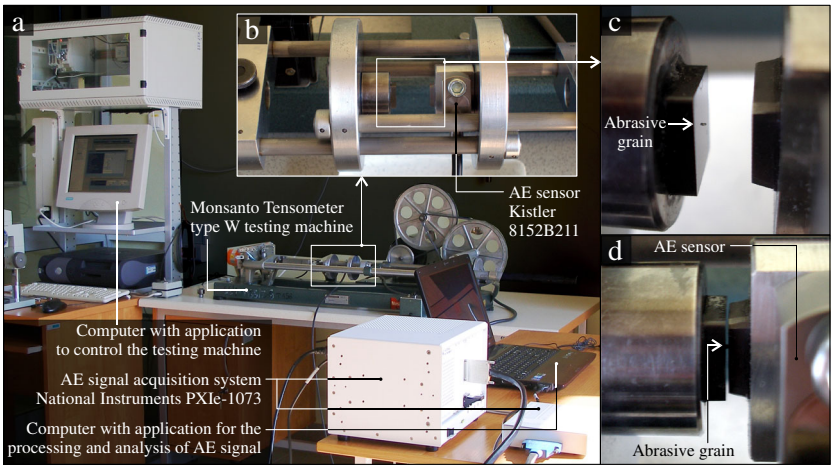

Fig. 5 Experimental stand for strength tests: **a** overall view, **b** view of the testing machine working zone, **c** view of gaping jaws with abrasive grain, and **d** view of the jaws before compression tests

out with the experiment being repeated three times for each kind of abrasive grain.

An overview of the technical roadmap for the described research process is presented in Fig. 6. The complete list of computing and experiment facilities is listed in Table 2.

3.2 Results and discussion

Figure 7 presents exemplary changes in the force registered during the static test for single-axis compression of the four types of abrasive grains within the function of time (Fig. 7a–d), as well as the values of the forces for which the grain decohesion occurred (Fig. 7e, f). Analysis of the average values of the compression force F_c, for which the decohesion of abrasive grains occurred (Fig. 7f), indicates that the least durable grain was white fused alumina ($F_{c\ av}$=32.7 N). The Abral® grains underwent decohesion with an average force value $F_{c\ av}$=42.0 N, while that of green silicon carbide was $F_{c\ av}$=53.3 N. The highest force values were measured in the microcrystalline sintered corundum SG™ grains during axial compression tests ($F_{c\ av}$=75.7 N). This means that the SG™ grain's static resistance, expressed with the compression force average value, is 230 % greater than that of the white fused alumina abrasive grains. As compared with 99A grains, Abral® and 99C grains were characterized by a resistance 128 and 163 % higher, respectively.

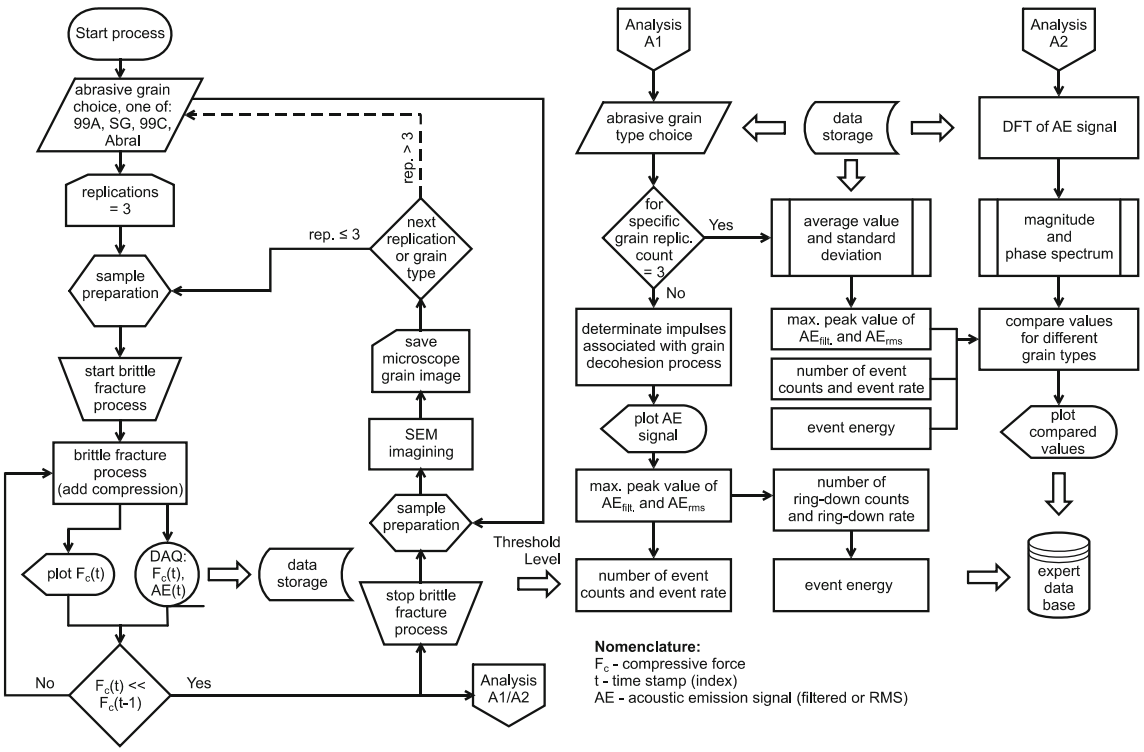

Fig. 6 Overview of the technical roadmap—concept map for the research process

It needs to be observed that the tests performed with the Abral® grains were characterized by the smallest result spread with reference to the compression force measurement. The standard result deviation of the tests carried out on 99C grains was over 50 % of the average compression force (Fig. 7f).

Table 2 The computing and experiment facilities (source: manufacturer or software company data sheets and brochures)

Name	Model/version	Manufacturer/company	Description
Modular instruments for height performance and flexible DAQ system			
PXI Express chassis	PXIe-1073	National Instruments (USA)	High-throughput backplane with triggering and tight synchronization, up to 250 MB/s per slot bandwidth
Multifunction DAQ	PXIe-6124/S Series	National Instruments (USA)	Simultaneous sampling multifunction DAQ with a dedicated AD converter per channel, ideal for ultrasonic industrial measurement and control, 4 simultaneously sampled analog inputs at 4 MS/s per channel with 16 bits of resolution
Shielded I/O connector block	SCB-68	National Instruments (USA)	Shielded I/O 68-pin connector block for DAQ devices, enables the easy addition of signal conditioning to the analog input, output and PFI signals
PXI Express Card	8360	National Instruments (USA)	Suitable for direct laptop control of PXI system, software transparent link that requires no programming, sustained throughput up to 110 MB/s
Acoustic emission sensor	8152B211	Kistler Instrument Corp. (Switzerland)	Piezotron™ sensor with an integral impedance converter for measuring acoustic emission (AE) in machine structures, a very high sensitivity for surface (Rayleigh) and longitudinal waves, bandwidth 100–900 kHz
Piezotron™ AE coupler	5125B2	Kistler Instrument Corp. (Switzerland)	Processes the high-frequency output signals from Kistler emission sensors; gain (×1), filters (HPF 50 kHz and LPF 1000 kHz) and RMS convert (time constant 1.2 ms)
Electron scanning microscope	JSM-5500LV	JEOL Ltd. (Japan)	Easily operable SEM, equipped with electron optics, specimen chamber (up to 150 mm) and stage for high magnification observation (up to 300,000 times) and imaging, resolution of 3.5 nm, operating at an accelerating voltage range of 0.5 to 30 kV (53 steps)
Resistance machine	Tensometer type W	Monsanto (Great Britain)	Universal testing machine used to evaluate the tensile properties of materials such as their Young's modulus or tensile strength, machine works either by driving a screw
Amplifier	MP85A	Hottinger Baldwin Messtechnik GmbH (Germany)	Two-channel measuring amplifier suitable for connecting the transducers, installed with PME Assistant software
Force transducer	RSCA C3/2t	Hottinger Baldwin Messtechnik GmbH (Germany)	Load cell with strain gauge measuring system, suitable for measuring tensile and compressive forces (static and dynamic measurements), maximum capacity 20 kN
Laptop	NP-R580-JS03PL	Samsung Corp. (South Korea)	Personal computer to control PXIe system, 4GB RAM, Intel i5 2.27 GHz, Windows 7 32 bit
Computing facilities			
LabVIEW	8.5	National Instruments (USA)	DAQ (data acquisition) system design software
DAQmx	9.0.2	National Instruments (USA)	Data AQuisition multifunction, high-performance, multithreaded driver
MAX	4.6.2	National Instruments (USA)	Measurement & Automation Explorer (MAX) provides access to DAQ devices; necessary to configure and conduct diagnostics upon National Instruments hardware
JEOL SEM software	JSM-5500LV	JEOL Ltd. (Japan)	Streamlines the imaging and analytical workflow, allowing simple point and shoot navigation across the sample surface for imaging and analysis
PME Assistant	2.0	Hottinger Baldwin Messtechnik GmbH (Germany)	Enables the setting of all the device parameters, allows for rapidly and easily produced measurement results with the MP85A
MATLAB®	2011b	The MathWorks, Inc. (USA)	The language of technical computing; used to analyze data and plot results

Due to the low sampling frequency of the force F_c sensor, the obtained results were complemented by a far more detailed analysis of the acoustic emission signals registered during the single-axis compression test of abrasive grains.

The piezoelectric sensors, such as the sensor type 8152B211 by Kistler Instrument Corp. used during the tests, are exceptionally sensitive to longitudinal waves (the vibrations occur in the direction consistent with the direction of its diffusion) and *Rayleigh's waves* (distortion propagating along the surface) [25]. These waves, being the result of rapid stress released by distortion sources, are propagated along the planar surface of the solid. In this way, the acoustic emission signal contains only the information concerning the elastic waves registered by the sensor, i.e., information on the intensity, energy, and other features of the single source or multiple sources at the same time. Figure 8 presents examples of the registered AE signals for the four examined grains.

On the basis of the registered AE signals, the maximum acoustic emission signal peak values (Fig. 9a) and their average values (Fig. 9b) were determined. The maximum amplitudes of the root mean square value of the acoustic emission signal were calculated (Fig. 10).

In order to isolate and describe single activated AE sources, the term AE events was introduced. In order to determine the event, it is assumed that a single event takes the shape of an underdamped sine wave—because of the energy loss, there is an attenuation of vibrations within the real/material center—and is the AE impulse. The event may be determined by estimating its envelope on the signal, e.g., using the Hilbert transform. In practice, it is assumed that the event lasts from the moment the ring-down appears (peak of the signal whose amplitude is higher than the discrimination level) and lasts until the moment when the ring-down no longer appears in the following time samples (Fig. 11). This means that a group of ring-downs that occur in subsequent samples are registered as an acoustic emission event and the whole event group as an acoustic emission signal in the registered time frame [26].

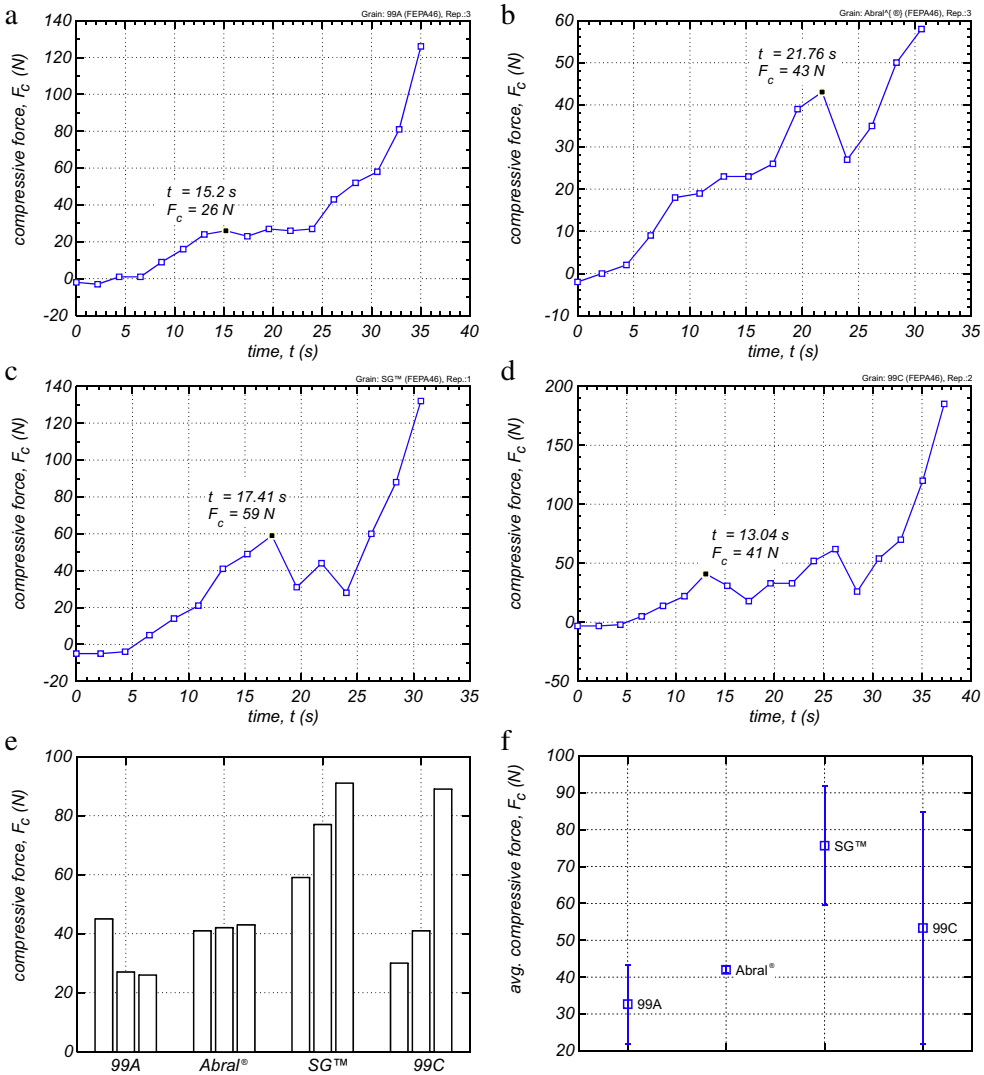

Fig. 7 Example of changes in the compressive force F_c registered during the static uniaxial compression tests of abrasive grains within a time function: **a** white fused alumina grains (99A), **b** aluminum oxynitride grains (Abral®), **c** microcrystalline sintered corundum grains (SG™), **d** green silicon carbide grains (99C) and compared with the compressive force values for moments of grain decohesion, **e** for subsequent repetitions, and **f** average values with symmetric *error bars* that are two standard deviation units

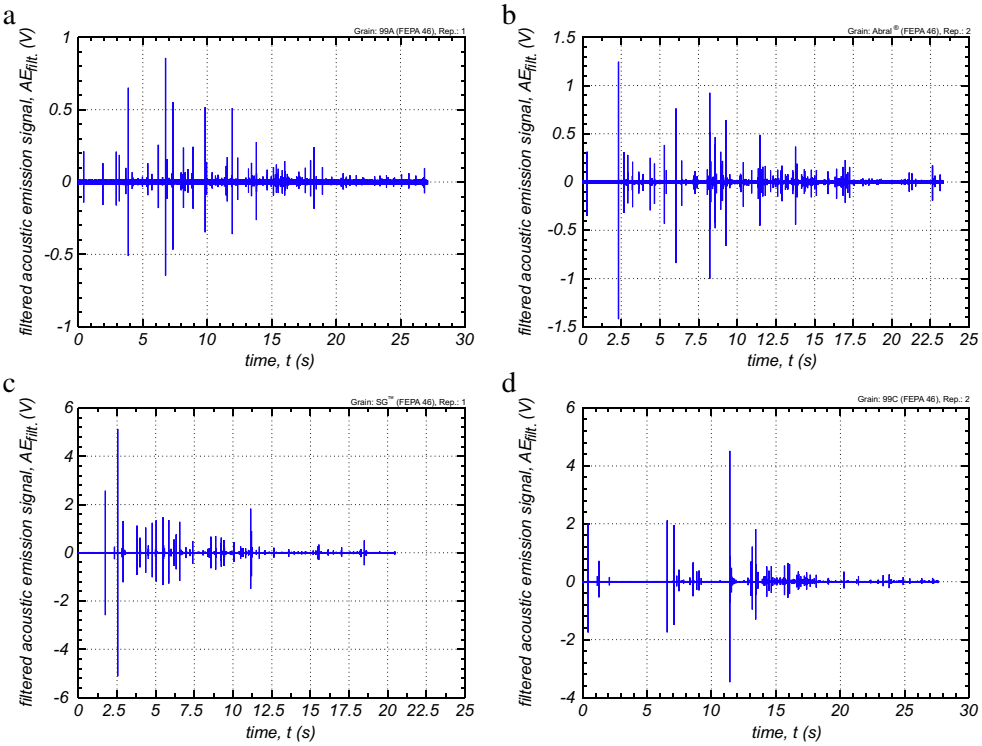

Fig. 8 Examples of acoustic emission-filtered raw signal ($AE_{filt.}$) registered during the static uniaxial compression tests of abrasive grains within a time function: **a** white fused alumina grains (99A), **b** aluminum oxynitride grains (Abral®), **c** microcrystalline sintered corundum grains (SG™), and **d** green silicon carbide grains (99C)

A threshold level U_g was adopted at the level of 10 mV when estimating the AE impulses and signal parameters.

Figures 12 and 13 present the number of counts (N_e) and the count rate (n_e) of events with an amplitude higher than the threshold level registered in the acoustic emission signal during the static test for the compression of various types of abrasive grains. Figure 14, on the other hand, presents parameter values determined for the maximum acoustic emission impulses registered during the compression test of the examined abrasive grains.

The results of the tests conducted indicate that the number of ring-down counts per single event (Fig. 14d, f) for each acoustic emission signal was relatively poorly connected to the AE energy function (Fig. 14e, g). The number of event counts N_e in the acoustic emission signal (Fig. 12) may, however, be a good measure of the cracking stages that altogether form the macroscopic process of abrasive grain destruction. What seems, however, to be most useful is the evaluation of the event rate measurement (Fig. 13). The event count rate n_e during propagation of the microfissure depends on the material microstructure and is proportional in relation to the crystal size and the intercrystalline distances [29]:

$$\frac{\mathrm{d}n_e}{\mathrm{d}t} \approx \frac{1}{G_m}\left(\frac{\mathrm{d}a}{\mathrm{d}t}\right), \tag{1}$$

where $\frac{da}{dt}$ is the fissure expansion rate and G_m is the average crystal size.

Moreover, the acoustic emission event count rate is connected with the direct stress intensity factor measure K_I, which determines changes in stress layout within the elastic material following the presence of cracking. Therefore, the higher the K_I value, which is the case in a large number of intergranular borders in which crystals have a different orientation toward

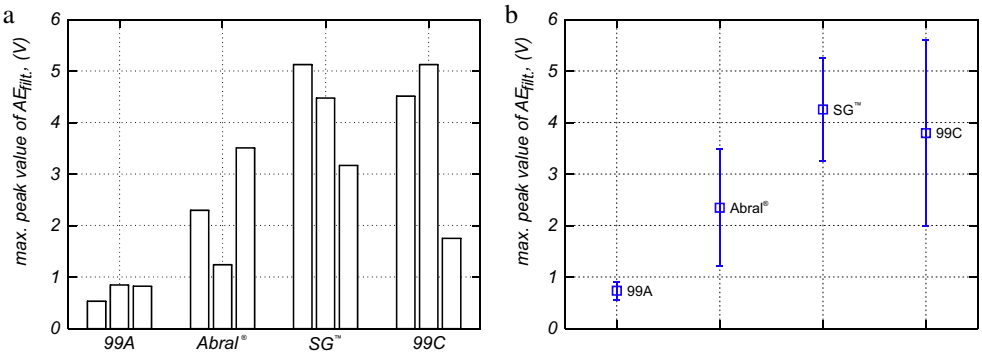

Fig. 9 Maximal peak values of acoustic emission-filtered raw signal ($AE_{filt.}$) registered during the static uniaxial compression tests of abrasive grains in time function: **a** the maximum values in subsequent repetitions and **b** average values of peaks with symmetric *error bars* that are two standard deviation units

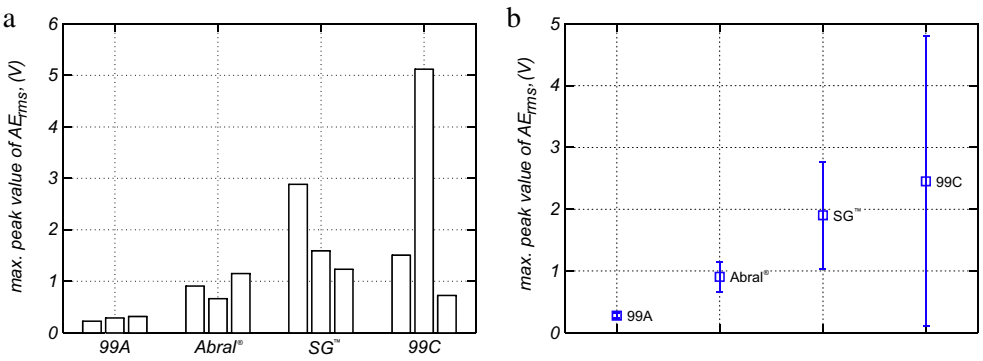

Fig. 10 Maximal amplitude of acoustic emission root mean square value (AE_{RMS}) registered during the static uniaxial compression tests of abrasive grains within a time function: **a** the maximum values in subsequent repetitions and **b** average values of peaks with symmetric *error bars* that are two standard deviation units

each other (as in the case of microcrystalline sintered corundum), the easier the propagation of existing fractures, as well as the creation of new ones, both of which lead to microchippings. This is confirmed by the SEM observations as presented in Fig. 15.

As far as their structure is concerned, abrasive grain types 99A and 99C and Abral® are a mixture composed of monocrystals (mainly 99C), crystallites, and crystal conglomerates combined into aggregates. Most probably, the dominant share of monocrystals in 99C grains causes their relatively high resistance and contributes to their characteristic fracture mechanism. The increased volume of 6H polytype in the grain leads to the occurrence of microparticle splintering upon the skid surfaces that run along the hexagonal layers, as confirmed by the characteristic fractures visible in the SEM views of the chipped grain (Fig. 15d).

The lowest values of the ring-down counts (Fig. 12), event count rate (Fig. 12), and event energy (Fig. 14g) for 99A grains may be indicative of the possible occurrence of the dislocation mechanism that increases resistance to fractures in the decohesion process. This phenomenon is characteristic of ionic crystals, for which, instead of the assumption of the existence of internal materials flaws, it is assumed that microfractures will appear during coalescence of the numerous edge dislocations in a single skid plane. This causes reduction of the stress around the microfracture. As a result, the fused alumina shows a transcrystalline fracture along the preferred cleavage planes (on the basic surface (001))—Fig. 15a.

The cleavable decohesion nature is most obviously dominant in the Abral® grains (Fig. 15c), as a result of which the examined parameters displayed values that were higher than in the case of 99A grains and lower in the case of the microcrystalline sintered corundum SG™ grains.

The tests in the frequency domain complement the knowledge of the grain cracking process in relation to a particular signal component frequency and, thus, allow for more detailed characteristics of the acoustic emission impulse's source to emerge. In the brittle fracture phenomenon analysis, the elastic waves provide important information on the way the subsequent grains that were subject to stress are damaged. As a result of the operation of stress forces, the fracture process, including the macro- and microfractures, may occur in different ways and with different energies. Monitoring and detailed diagnostics of the stress waves, that are the result of subsequent stages of abrasive grain decohesion, may constitute the perfect tool for describing the fracture mechanism and also provide information concerning the material resistance to brittle fracture. It is expected that on basis of properly directed signal time-frequency analysis, differences in the speed and value of the released energy may be indicated.

For the need of analysis of the registered acoustic emission signals in the single-axis test of selected abrasive grains'

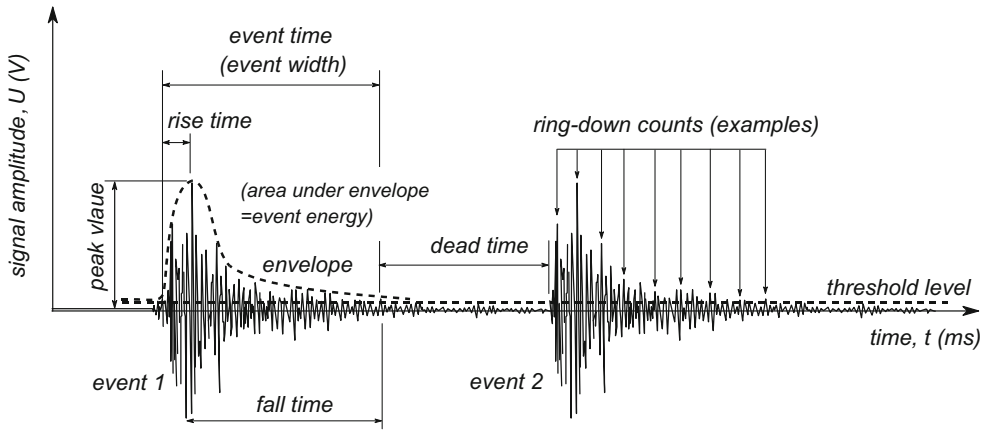

Fig. 11 Selected parameters of acoustic emission events (authors own study on the basis of [26–28])

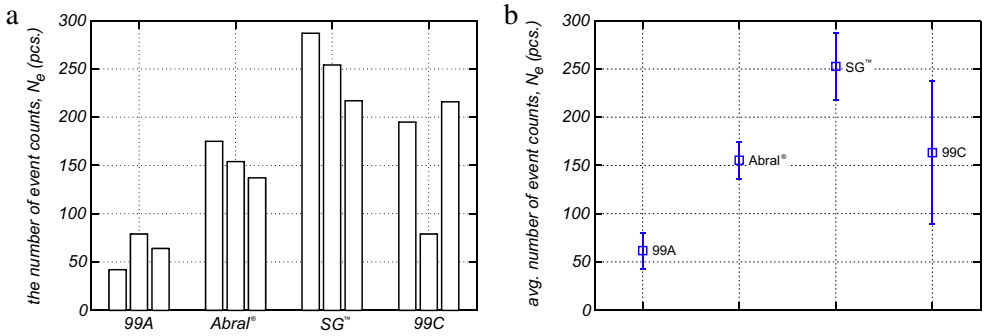

Fig. 12 A comparison of a number of event counts (N_e) with an amplitude greater than the threshold level (0.01 V) observed in acoustic emission signals from the static uniaxial compression tests for different abrasive grain types: **a** the number of event counts in subsequent repetitions and **b** average values of the number of event counts with symmetric *error bars* that are two standard deviation units

compression, frequency analyses were carried out using discrete Fourier transforms (Figs. 16, 17, 18, and 19). This is the most popular and universal method of signal analysis in the frequency domain [30]. The graphs present the harmonic magnitudes in the range of 1–1250 kHz, both in the linear scale (Figs. 16a, 17a, 18a, and 19a) and the logarithmic scale (Figs. 16b, 17b, 18b, and 19b), as well as the change of the phase angle (Figs. 16c, 17c, 18c, and 19c) and the signal spectrogram for the whole period of acoustic emission impulse duration (Figs. 16d, 17d, 18d, and 19d). This data was obtained on basis of the signals registered for the four types of abrasive grains.

Analysis of the research results presented in Figs. 16, 17, 18, and 19 points to the typical properties of exponentially damped impulses, i.e., the relatively low content of the harmonics with high frequencies (exceeding half of the analyzed frequency range) and the characteristic transition toward lower and lower frequency components. After the abrupt energy release, the stress waves undergo damping and dispersion in their propagation center. The amplitude spectrum charts obtained are therefore characteristic of low-pass signals for which the spectral density drops to zero as the angular frequency increases to infinity. Therefore, in the averaged analysis, carried out using Fourier transform, there is a clear majority of low frequencies (50-500 kHz). The harmonics ranging from 100 to 400 kHz have the greatest intensity. In this range, the predominant components are 120, 240, and 360 kHz.

Moreover, the registered signals are characterized by broadband phase modulation (PM)—the carrier wave is modulated in a wide frequency spectrum and sent during the impulse occurrence. As the phase of the particular components is of negative value which is at the same time inversely proportional to the harmonics, each subsequent signal component is delayed in relation to the previous one. As the brittle fracture mechanism may be different but concerns the same narrow group of ceramic materials, the analyses carried out did not indicate any unambiguous differences between the particular grains.

The measurement results of the acoustic emission signal and frequency domain analysis suggest a high dependence of the amplitude on K_{Ic} of individual grains, which is associated with the propagation of unstable cracks in the AlON and 99A grains at much lower loads than for SG™ grains.

Analyzing a single harmonic for grain type 99A, we can determine that the largest magnitude value $|Y(f)|$ is 125 kHz, but other harmonics (up to 500 kHz) are also significant, for example, 250 and 300 kHz. The most important bandwidth seems to be from 125 to 375 kHz, with damping of signal value by up to 10 times (−20 dB)—Fig. 16b. Harmonics with a damping volume of a hundred times (-40 dB) are in bandwidth 375 to 900 kHz. Low frequencies remain the longest

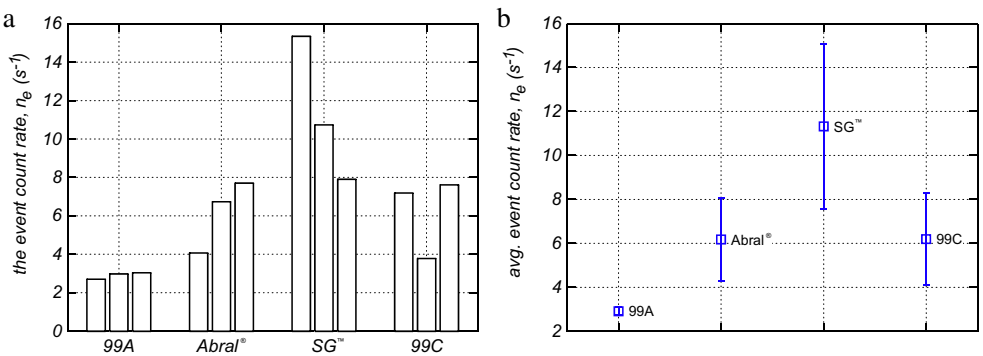

Fig. 13 A comparison of the event count rates (n_e) for events observed in an acoustic emission signal during the static uniaxial compression tests for different abrasive grain types: **a** the event count rate in subsequent repetitions and **b** average values of the event count rate with symmetric *error bars* that are two standard deviation units

duration in signal time-frequency representation, which can be observed by a spectrogram—Fig. 16d. This dynamic analysis shows that almost all frequencies are damped in a quick and hard way. After 2 ms, the power of the signal is damped over 10^7 times (−70 dB or more). These unfavorable conditions are confirmed by a characteristic of the phase angle (Fig. 16c). The linear decrease of the phase indicates an acoustic emission impulse as FIR filter, which is usually designed to be linear phase. The function of frequency is a straight line. This results in a delay through all frequencies.

For aluminum oxynitride grain (Fig. 17a), the largest magnitude value $|Y(f)|$ is about 100 kHz, but the value is 1.5 larger in relation to the 99A grain. The amplification or the damping in decibel scale (Fig. 17b, d) is similar to previous cases.

In the case of microcrystalline sintered corundum grains (Fig. 18a), the largest magnitude value $|Y(f)|$ is about 100 kHz (like for Abral® grain), but that value is now 10 times larger in relation to the 99A grain and 6.5 times in relation to Abral® grain. The range of significant harmonics is similar to other grains, but the damping factor is different (Fig. 18b). The

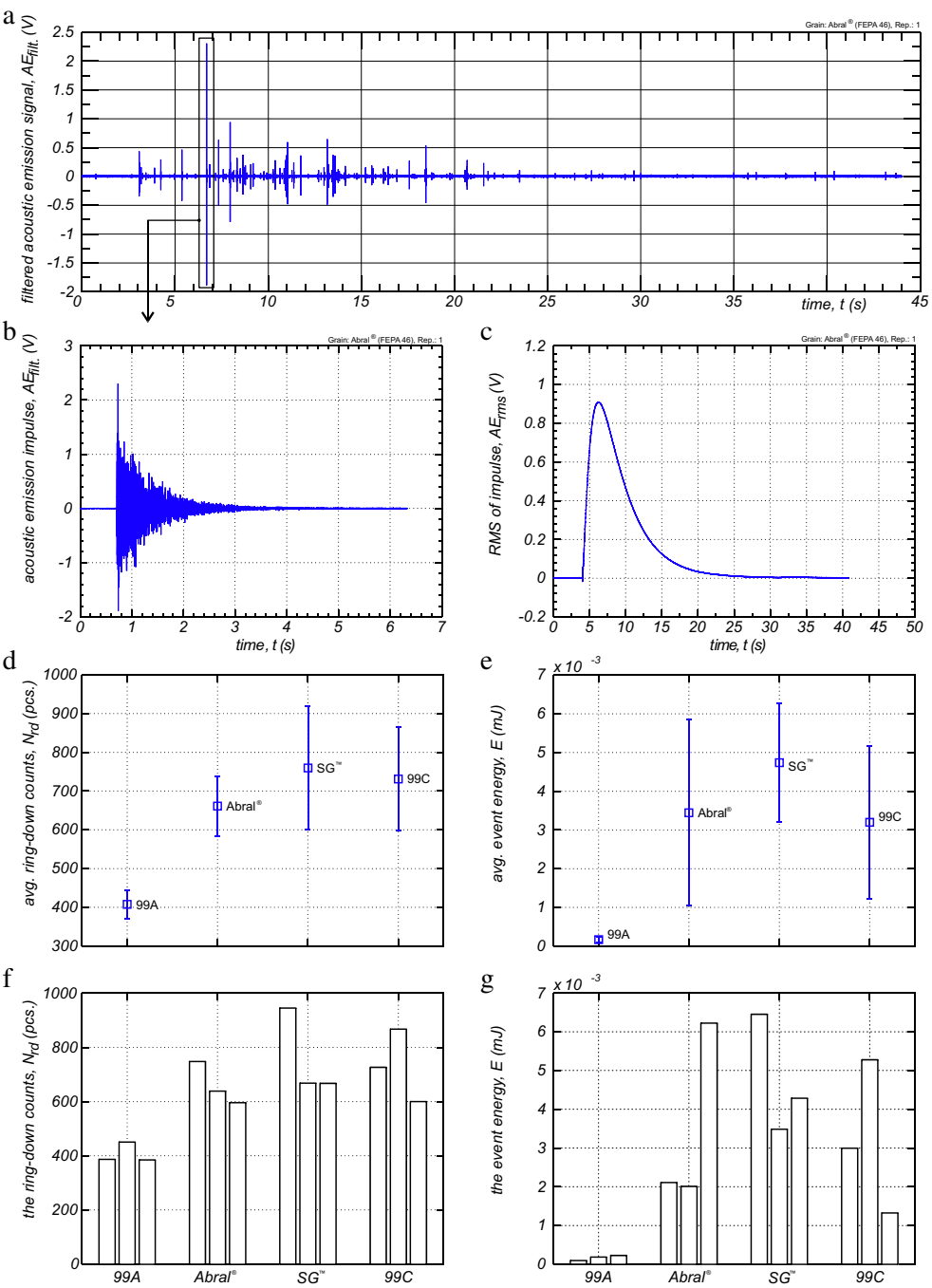

Fig. 14 Parameters for single acoustic emission impulses registered during the static uniaxial compression tests for different abrasive grain types: **a** an example of a raw acoustic emission signal for aluminum oxynitride grains (Abral®); **b** a single impulse with maximal peak value within the registered signal; **c** root mean value of the impulse calculated by AE Piezotron coupler (type 5125B2, Kistler Instrument Corp.); **d**, **f** the number of ring-down counts for the analyzed grains; **e**, **g** event energy for the analyzed grains

values for low frequencies, up to 400 kHz, are significant on the positive side (up to +30 dB) of the scale. It means that the signal has an amplification factor. The signal is damped 10 times (−20 dB) only for 900 kHz or more. This situation is reflected in the spectrogram (Fig. 18d), where we can see harmonics with higher values for a longer duration.

The last type of grain (green silicon carbide, 99C) has the highest value for 125 kHz (like for grain 99A type)—Fig. 19a. The other features in frequency response seem to be similar to the results obtained for aluminum oxynitride grain.

The microstructural condition of each abrasive grain (as microblades in the grinding process) will generate different signals from the grinding zone. Relative changes in the amplitude and duration of the AE signals responsive to the varied phenomena of wear, in both macro- and nanoscales, are closely related to the scope and speed of crack promotion. It follows that the optimization of the grinding process due to the size of the load and grain microstructure determines the beneficial wear mechanism of AlON grains and enables the use of the specific properties of the grains (such as limiting wetting by steel).

4 Conclusions

The creation and registration of the acoustic emission signals in different kinds of abrasive grains during compression tests made it possible to track the fracture processes occurring within the macro- and microscopic scales. Depending on the abrasive grain structure, acoustic signal emission with varied amplitude was obtained. The time structure of the AE signal depends then on the course of the abrasive grain destruction process.

The experimental tests conducted demonstrate that the methodology presented enables the registration of phenomenon occurring in the stress field, connected with the abrasive grain microstructure. The most important results include the following:

– Showing resemblances in the nature of abrasive grain brittle fractures visible in the microscopic images, especially in the case of AlON (Abral®) and SG™.
– Proving that another force is necessary for decohesion of abrasive grains made from different materials, even though

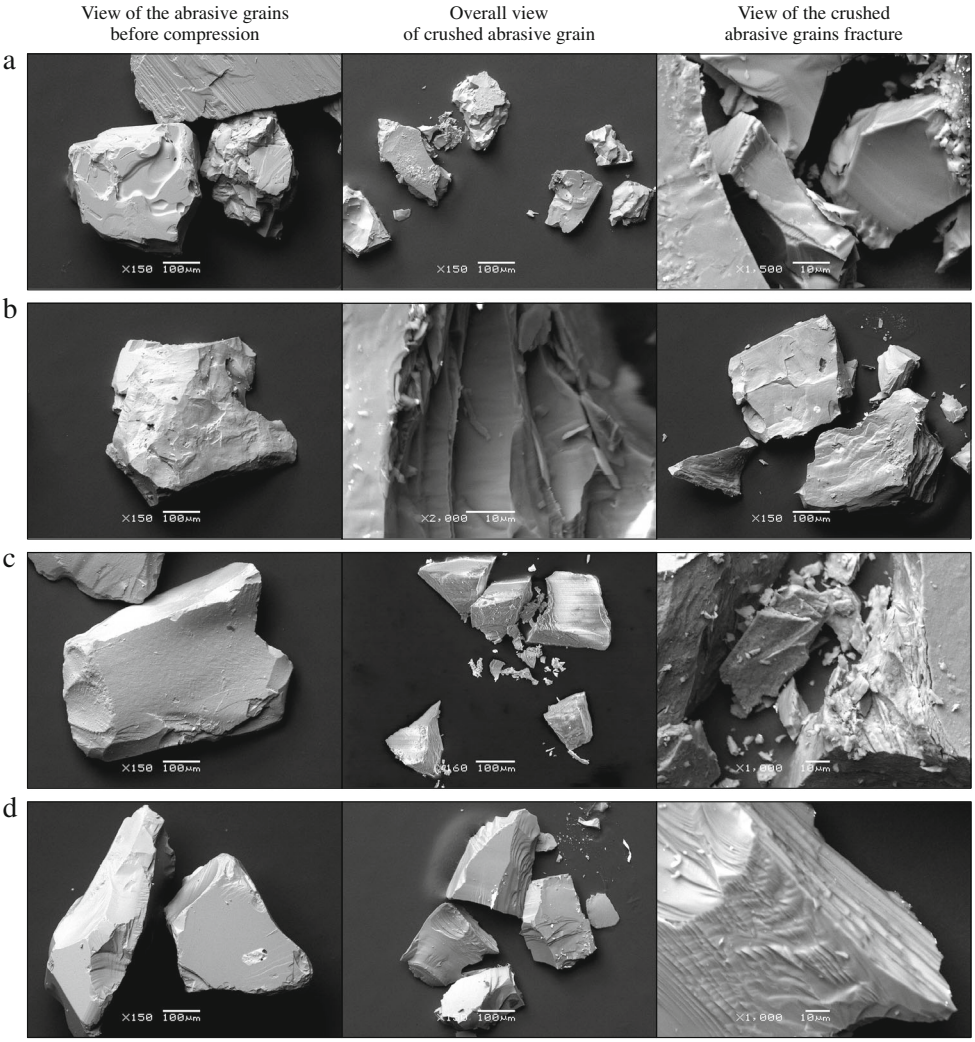

Fig. 15 SEM images of abrasive grain number 46 before compression testing and views of crushed grains: **a** white fused alumina 99A, **b** aluminum oxynitride Abral®, **c** microcrystalline sintered corundum SG™, and **d** green silicon carbide 99C

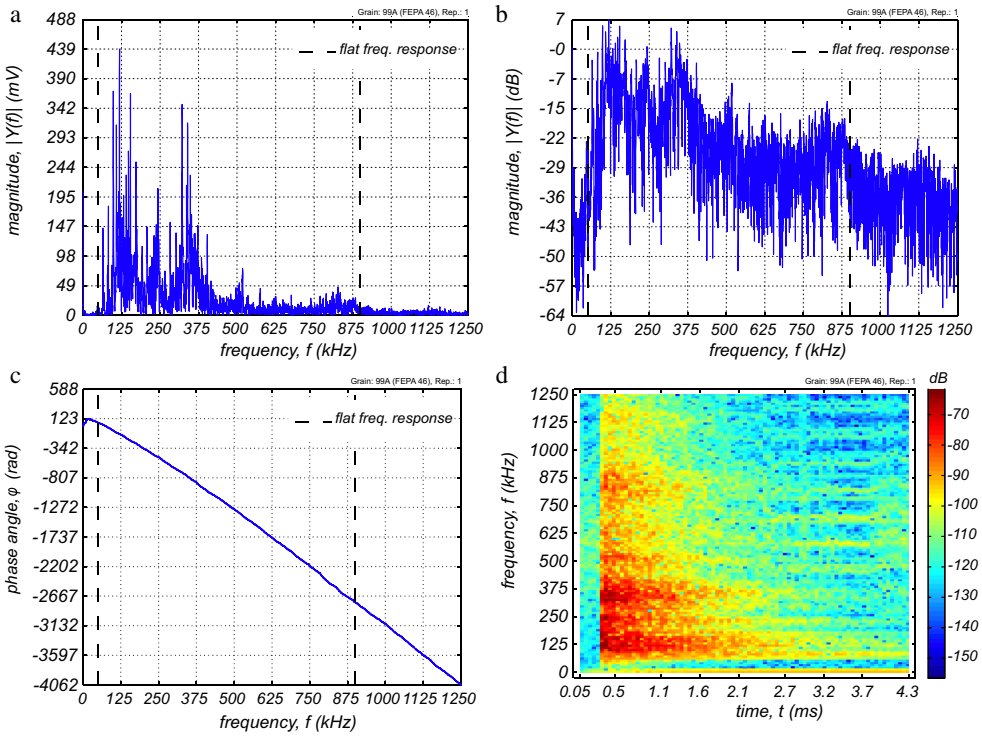

Fig. 16 Example of acoustic emission impulse frequency characteristics for white fused alumina grain (99A): **a** frequency spectrum in linear scale (discrete Fourier transform, $DFT_{NFFT}=2^{14}$), **b** frequency spectrum in decibel scale, **c** phase spectrum of signal (in radians), and **d** spectrogram of signal (window type—Hamming, window size—256 samples, overlap of segments—50 %)

all of the analyzed grains belong to one group of ceramic materials.

– Determining the level of destructive stress which equals 42 N for aluminum oxynitride grains, proving that the only grains more resistant than Abral® grains are SG™ grains, which is especially visible when considering the measurement results spread.

– Showing the differences between the AE signals registered during the compression tests of various abrasive grain types and thus pointing to the possibility of differentiating

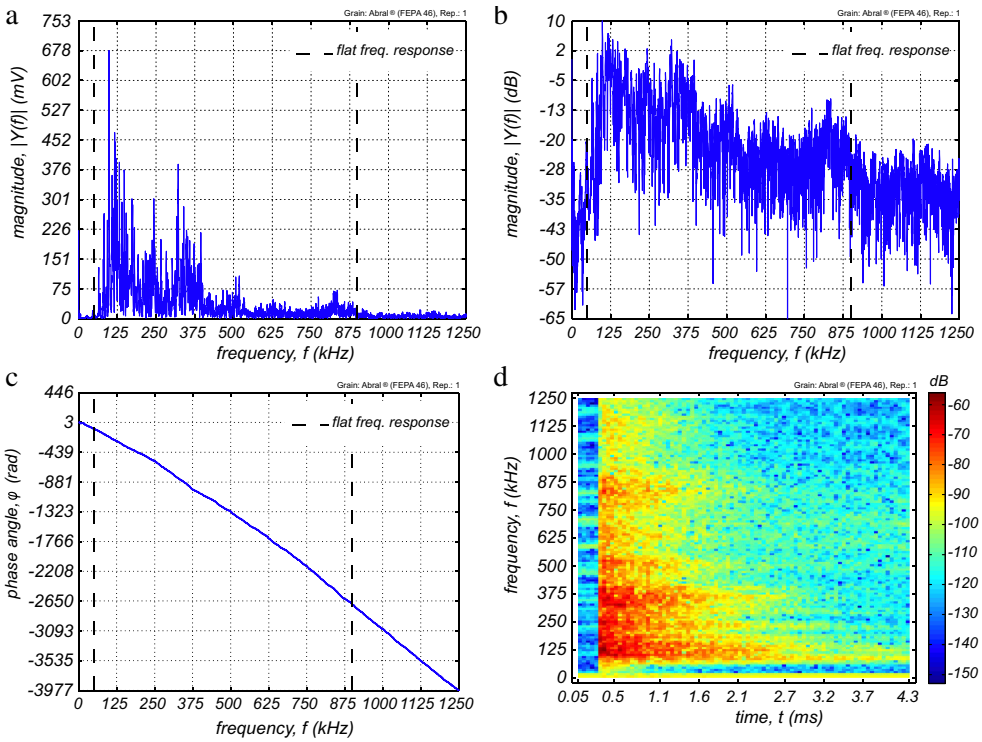

Fig. 17 Example of acoustic emission impulse frequency characteristics for aluminum oxynitride grains (Abral®): **a** frequency spectrum in linear scale (discrete Fourier transform, $DFT_{NFFT}=2^{14}$), **b** frequency spectrum in decibel scale, **c** phase spectrum of signal (in radians), and **d** spectrogram of signal (window type—Hamming, window size—256 samples, overlap of segments—50 %)

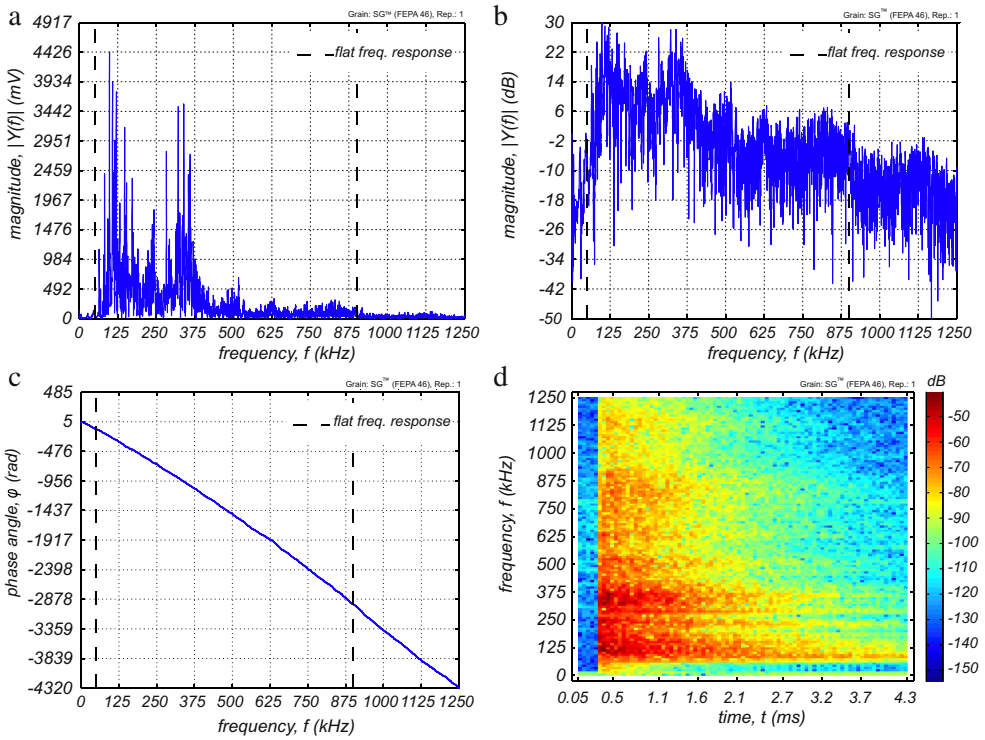

Fig. 18 Example of acoustic emission impulse frequency characteristics for microcrystalline sintered corundum grain (SG™): **a** frequency spectrum in linear scale (discrete Fourier transform, $DFT_{NFFT}=2^{14}$), **b** frequency spectrum in decibel scale, **c** phase spectrum of signal (in radians), and **d** spectrogram of signal (window type—Hamming, window size—256 samples, overlap of segments—50 %)

between grains using the stress-wave emission (SWE) analysis method. This is especially relevant in the case of three types: 99A, Abral®, and SG™. Each of these grain types is characterized by increasing the number of ring-down counts and event count rate (in this order).

- The event count rate, due to its direct connection with the grain crystalline structure and their resistance to brittle fracture, is a particularly effective evaluation parameter.
- Analysis of the number of ring-down counts in the AE events and their energy identifies only two grain groups:

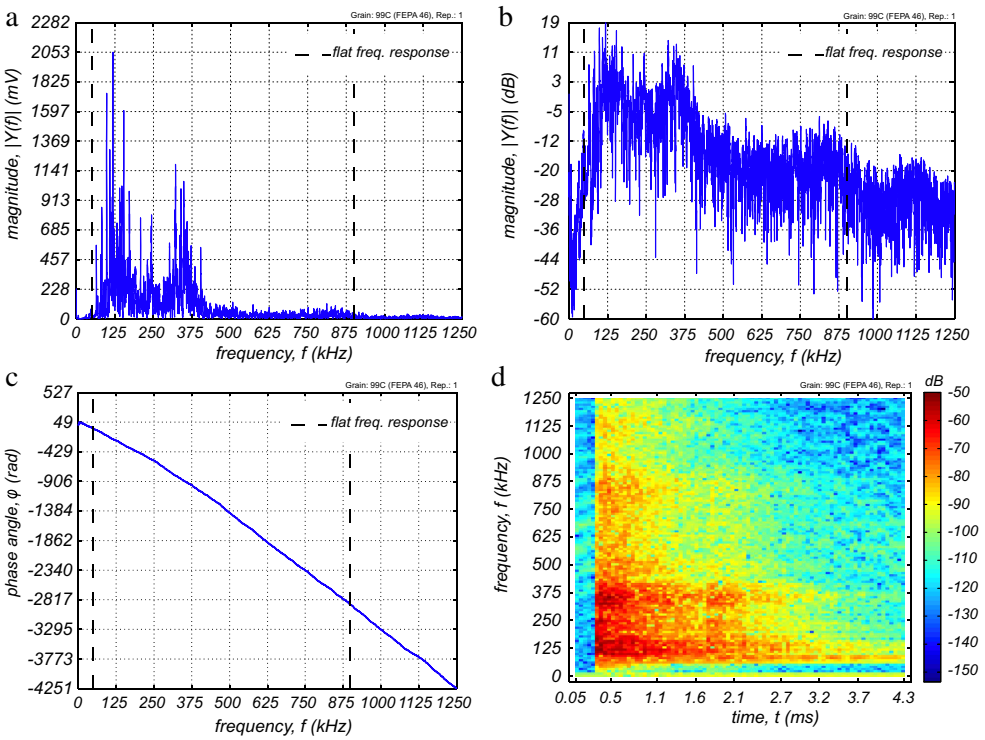

Fig. 19 Example of acoustic emission impulse frequency characteristics for green silicon carbide grains (99C): **a** frequency spectrum in linear scale (discrete Fourier transform, $DFT_{NFFT}=2^{14}$), **b** frequency spectrum in decibel scale, **c** phase spectrum of signal (in radians), and **d** spectrogram of signal (window type—Hamming, window size—256 samples, overlap of segments—50 %)

those with relatively low energy and number of ring-down counts (99A) and those grains with many stages of fracture occurring and increasingly greater energy.
– No unanimous differences between the AE signals analyzed in the frequency domain.

What should be determined in future tests are the stress levels that correspond to the start of the stable fracture development phase and above which the microfractures start to grow to critical size. The efficiency of tests concerning the application of acoustic emission as a measurement method is very much dependent on the proper selection of the signal processing method and chaining. Solutions to those problems connected with acoustic diagnostic control require further development to perfect the methods of detection and localization of the sources of the registered stress waves, induced by material demages.

The results described are one of the stages for creating expertise, which may in the future be used in practical applications. The conclusions of the work relate to basic research in the form of the experimental work undertaken primarily to acquire knowledge about the phenomenon of acoustic emission observable during the destruction of the abrasive grains. The isolation and study of individual events and the nonaggregated form of the acoustic emission signal will help in the development of an effective diagnostic tool. This knowledge can be used in the future to develop monitoring methodology of the grinding process involving grinding wheels made of AlON abrasive grains and other abrasives included in the reported studies (99A, SG™, 99C).

The authors recommend that further acoustic emission signal tests, especially the power density spectrum estimation, be carried out using such methods as Burg's method [31, 32], Welch's method [32], or other autoregression methods [32]. What could also be introduced into the analyses is calculating the spectrum using the chirp Z-transform algorithm [33, 34] or the mel-frequency cepstrum analysis (MFC) [35, 36]. Each of these methods expands analysis in the frequency domain and may be a source of valuable information on the registered signals. The authors have attempted using these aforementioned methods and the results of these analyses will form the subject of subsequent publications.

Compliance with ethical standards

Funding This study was not funded by any grant.

Conflict of interest The authors declare that they have no conflict of interest.

References

1. McCauley JW, Corbin ND (1980) Process for producing polycrystalline cubic aluminum oxynitride. US Patent No. 4241000
2. Mathers JP, Wood WP (1988) Aluminum nitride/aluminum oxynitride/group IVB metal nitride abrasive particles derived from a sol-gel process. US Patent No. 4788167
3. Mathers JP, Wood WP, Forester TE (1990) Aluminum oxide/aluminum oxynitride/group IVB metal nitride abrasive US particles derived from a sol-gel process. Patent No. 4957886
4. Dubots D, Faure P (1994) Process for direct nitriding of metals of low melting point. US Patent No. 5314675
5. Dubots D, Faure P (1994) Abrasive and/or refractory products based on melted and solidified oxynitrides and process preparing the same. US Patent No. 5336280
6. Galvin HP (1995) Abrasive material. France Patent FR2720391
7. Sutton S (2000) What's new in abrasives. Ceramic industry. http://www.ceramicindustry.com/articles/87534-what-s-new-in-abrasives. Accessed 20 Jan 2015
8. Alteo (2015) La Bâthie. http://alteo-alumina.com/en/la-bâthie. Accessed 25 Jan 2015
9. Rio Tinto Alcan Inc. (2007) Our history. http://www.riotintoalcan.com/ENG/whoweare/28.asp. Accessed 20 Jan 2015
10. Rio Tinto Alcan Inc. (2013) History. http://www.riotinto.com/aboutus/history-4705.aspx. Accessed 20 Jan 2015
11. Bourlier F (2005) Abrasive particles based on aluminium oxynitride. US Patent Application Publication No. 2005/0160678 A1
12. Klocke F (2009) Manufacturing processes 2: grinding, honing, lapping, 2009th edn. Springer, Berlin
13. Alteo (2014) Alteo fused alumina more than 100 years of expertise. http://alteo-alumina.com/sites/default/files/Ressources/ALTEO%20Fused%20Aluminas%20Brochure_2.pdf. Accessed 25 Jan 2015
14. Cardarelli F (2008) Materials handbook. Springer, London
15. Jackson MJ, Davim JP (2010) Machining with abrasives, 2011th edn. Springer, New York
16. Mole Abrasivi Ermoli SRL "LA" grinding wheels in ABRAL corundum. http://www.ermoli.it/eng/prodotti/LA grinding wheels in Abral corunduml.pdf. Accessed 18 Jan 2012
17. Rappold E (2005) Schleifbrand im Griff. WB Werkstatt + Betrieb 09:156–159
18. Roquefeuil F (2001) Abral: a new electrofused aluminum oxynitride abrasive grain for precision grinding. Precision grinding & finishing in the global economy—2001 conference proceedings. Gorham, 10/1/2001, Oak Brook
19. Kopac J, Krajnik P (2006) High-performance grinding—a review. J Mater Process Technol 175:278–284. doi:10.1016/j.jmatprotec.2005.04.010
20. Krajnik P, Kopac J (2005) Empirical modelling and optimisation of precision grinding. In: Kuljanic E (ed) AMST'05 advanced manufacturing systems and technology. Springer, Vienna, pp 201–210
21. Roquefeuil F (2003) Abral: a new approach to precision grinding. Abrasive Magazine
22. Roquefeuil F (2003) Abral: une nouvelle approche de la rectification. Mach Prod 780:II–VII
23. Webster J, Tricard M (2004) Innovations in abrasive products for precision grinding. CIRP Ann Manuf Technol 53:597–617. doi:10.1016/S0007-8506(07)60031-6

24. Jupiter Infomedia Ltd. (2005) Thermal damage in grinding course. http://articles.jimtrade.com/1/77.htm. Accessed 18 Jan 2012
25. Kistler Instrument Corporation (2007) Acceleration. Piezotron® sensor. Acoustic emission sensor. http://www.intertechnology.com/Kistler/pdfs/Accelerometer_Model_8152B.pdf. Accessed 02 Feb 2015
26. Mindess S (2004) Acoustic emission methods. In: Malhotra VM, Carino NJ (eds) Handbook on nondestructive testing of concrete, 2nd edn. CRC, Boca Raton, pp 16.1–16.17
27. Mansurov VA (1994) Acoustic emission from failing rock behaviour. Rock Mech Rock Engng 27(3):173–182
28. Carpinteri A, Lacidogna G, Niccolini G (2008) Multidimensional approaches to study Italian seismicity. In: Carpinteri A, Lacidogna G (eds) Acoustic emission and critical phenomena—from structural mechanics to geophysics. Taylor & Francis, London, pp 245–268
29. Ranachowski J, Rejmund F (1993) Acoustic emission in the brittle fracture process of ceramics. Institute of Fundamental Technological Research Polish Academy of Sciences (in Polish)
30. Sundararajan D (2001) The discrete fourier transform: theory, algorithms and applications. World Scientific, Singapore
31. Bos R, de Waele S, Broersen PMT (2002) Autoregressive spectral estimation by application of the Burg algorithm to irregularly sampled data. IEEE Trans Instrum Meas 51:1289–1294. doi:10.1109/TIM.2002.808031
32. Stoica P, Moses RL (2005) Spectral analysis of signals, 1st edn. Prentice Hall, Upper Saddle River
33. Rabiner LR, Gold B (1975) Theory and application of digital signal processing. Prentice Hall, Englewood Cliffs
34. Rabiner L, Schafer RW, Rader CM (1969) The chirp z-transform algorithm. IEEE Trans Audio Electroacoust 17:86–92. doi:10.1109/TAU.1969.1162034
35. McLoughlin I (2009) Applied speech and audio processing: with Matlab examples, 1st edn. Cambridge University Press, Cambridge
36. Selouani S-A (2011) Speech processing and soft computing. Springer, New York